



# A deep learning framework for gridding daily climate variables from a sparse station network

Alexandru Dumitrescu<sup>1</sup>

5 <sup>1</sup>Department of Climatology, Meteo Romania (National Meteorological Administration), Bucharest, 013686, Romania

*Correspondence to:* Alexandru Dumitrescu (dumitrescu@meteoromania.ro)

**Abstract.** High-resolution gridded climate datasets are essential for Earth system modelling and impact assessments, yet generating them from sparse, irregularly distributed station networks remains a significant challenge, particularly in regions with complex topography. This study evaluates the Spatial Multi-Attention Conditional Neural Process (SMACNP), a probabilistic deep learning framework, for the daily spatial interpolation of air temperature and precipitation, marking the first application of its localized encoder variant to the challenge of gridding climate data from a sparse station network. We investigate two distinct encoder configurations—Global and Localized—to determine the optimal structural prior for capturing spatial dependencies in data-scarce regimes. The models were developed and evaluated using data from a sparse network of meteorological stations in Romania from 2020 to 2023. To ensure applicability for long-term historical reconstruction, the input features were restricted to static topographic predictors derived from a Digital Elevation Model (DEM). Performance was benchmarked against Regression Kriging (RK), a standard geostatistical baseline that incorporates these same topographic covariates. Results demonstrate that the SMACNP architectures substantially outperform the RK baseline for both variables. The SMACNP (Localized) configuration, which utilizes an attention mechanism, emerged as the most robust model, achieving the lowest Mean Absolute Error (MAE) and the highest correlation across the majority of seasons. The performance gains were particularly pronounced for precipitation, where the deep learning models effectively captured fine-scale spatial heterogeneity and non-linearities that traditional methods tended to over-smooth. Furthermore, the SMACNP framework demonstrated superior uncertainty quantification; while RK exhibited significant overconfidence in precipitation estimates, the SMACNP (Localized) model produced well-calibrated probabilistic predictions with near-ideal empirical coverage. These findings indicate that localized neural process-based models offer a powerful, scalable, and physically plausible alternative to geostatistical methods for generating high-quality gridded climate datasets in complex, data-sparse environments.

## 1 Introduction

Daily gridded climate datasets are essential inputs for a wide range of models and impact assessments. Producing these fields from sparse, irregularly distributed station networks remains challenging, especially over complex terrain (Hijmans et al.,



30 2005). Air temperature tends to vary smoothly with controls such as elevation and latitude, whereas precipitation is  
intermittent, highly skewed, and spatially and temporally discontinuous (Daly et al., 1994). This problem is particularly  
critical in areas characterized by complex topography, where local factors like elevation and wind exposure introduce  
nonstationary relationships and heterogeneous spatial dependencies that challenge traditional geostatistical assumptions  
(Diggle and Ribeiro, 2007). Classical interpolators such as inverse distance weighting and kriging—including regression  
35 kriging (RK)—are widely used baselines (Hengl et al., 2007; Li and Heap, 2014). Their performance can degrade where  
covariance structure is nonstationary or relationships with covariates are nonlinear, conditions common in topographic-  
complex regions. While machine-learning approaches, particularly tree ensembles such as random forest and gradient  
boosting, often improve accuracy by leveraging rich covariates (e.g., satellite products, elevation, and reanalysis fields), they  
can still be limited in modeling the most complex spatial dependencies (Appelhans et al., 2015; Iwase and Takenawa, 2024;  
40 Sekulić et al., 2021).

Deep learning (DL) provides a powerful alternative, offering flexible, data-driven representations capable of modelling the  
complex spatial and temporal non-linear relationships inherent in climate data (Reichstein et al., 2019). Conditional Neural  
Processes (CNPs), for instance, learn distributions over functions from context points while providing uncertainty estimates  
(Garnelo et al., 2018). The convolutional variant, the Convolutional Conditional Neural Process (ConvCNP), uses  
45 translation-equivariant, continuous convolutions to capture local spatial dependencies and is well suited to gridded queries  
(Gordon et al., 2019; Vaughan et al., 2022). Attentive Neural Processes build on this by introducing cross-attention from  
target queries to context points, improving the handling of heterogeneity among observations (Kim et al., 2019). In parallel,  
Transformers—originating in natural language processing and later adapted to vision—provide a direct solution for  
leveraging rich covariate information from irregularly spaced stations. They use attention so each element can weight all  
50 others when forming its representation (Dosovitskiy et al., 2020; Vaswani et al., 2017). In spatial problems, this means that  
when geographic coordinates and relevant covariates (e.g., elevation) are encoded, a query at a target location can up-weight  
both nearby and distant stations that are most informative (e.g., those at similar elevation), directly addressing a key  
weakness of traditional distance-based interpolators. The Spatial Multi Attention Conditional Neural Process (SMACNP)  
exemplifies this approach by combining cross-attention from target queries to context stations with specialized spatial and  
55 feature-wise attention to capture distance-dependent structure and predictor correlations for interpolating point  
measurements (Bao et al., 2024b). Building on this, Gridded Transformer Neural Processes (GriddedTNP) were recently  
introduced to tackle the scalability issues of Transformer Neural Processes (TNPs) for large, unstructured spatio-temporal  
datasets like weather data, by employing specialized gridded pseudo-tokens for efficient attention (Ashman et al., 2024).  
Similarly, Graph Neural Processes (GNPs) combine Graph Neural Networks (GNNs) with Neural Processes (NPs) to  
60 explicitly model relationships and dependencies defined by a graph structure (Carr and Wingate, 2019). Taking a different  
structural approach, (Bao et al., 2024a) introduced a two-stage framework, the Location Embedded Graph Neural  
Networks–Residual Neural Processes (LEGNN-RNP), in which a Graph Neural Network is enhanced by a self-attention-



based location embedding generates an initial prediction, and a subsequent Residual Neural Process models the spatial patterns in the resulting errors, refining the final prediction and quantifying uncertainty in a manner similar to RK.

65 Despite these architectural advancements, the application of such probabilistic deep learning frameworks to extremely sparse observation networks in regions with complex topography remains under-explored. Our preliminary experiments in this specific context revealed that alternative architectures, such as the ConvCNP and GriddedTNP, struggled to generalize effectively when relying solely on static topographic predictors. Consequently, in this study, we evaluate SMACNP configured with global and localized encoders for the daily spatial interpolation of very sparse station-based climate  
70 variables. To the best of our knowledge, this represents the first application of the SMACNP architecture—specifically its localized encoder variant—to the challenge of gridding daily climate data from sparse observation networks. Their performance is compared with the RK method, which serves as the baseline, for the period 2020–2023. Particular emphasis is placed on interpolation accuracy and its associated uncertainty. The remainder of this paper is structured as follows. Section 2 describes the datasets employed and the preprocessing procedures. Section 3 outlines the methodological  
75 framework, including a detailed description of RK and SMACNP, and presents the experimental setup. Section 4 reports the results, with a focus on interpolation accuracy and predictive uncertainty. Finally, Section 5 and 6 discuss and summarize the main findings and provide concluding remarks. Our focus is on spatially aware probabilistic DL models (SMACNP and its variants) that natively handle irregular station sets and provide calibrated uncertainties. We therefore use RK as the geostatistical reference and do not benchmark tree-ensemble methods here.

## 80 **2 Study area and data**

The study is conducted over Romania, a region characterized by complex topography including the Carpathian Mountains, plateaus, and plains. We use daily meteorological station data and a topographic variable extracted from high-resolution Digital Elevation Model (DEM) to develop and evaluate the interpolation models

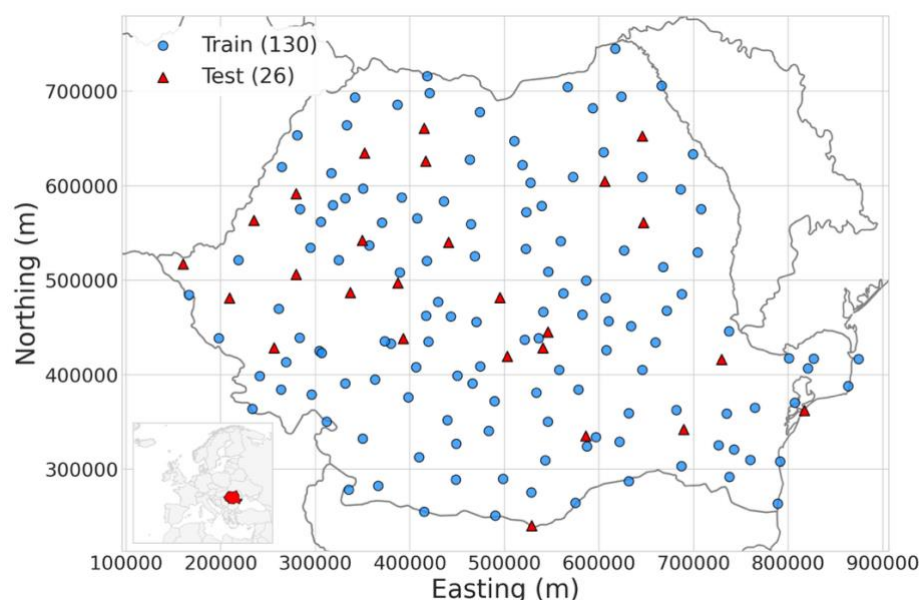
### **2.1 Meteorological and topographic datasets**

85 The primary dataset consists of daily homogenized mean air temperature (°C) and total precipitation (mm) from a network of meteorological stations across Romania, spanning 2020–2023. The complete dataset and associated station metadata can be accessed through the Zenodo repository (Dumitrescu, 2025). While the experiments in this study are conducted on this recent period, the proposed method is ultimately intended for application to the full long-term dataset covering 1901 to the present (Dumitrescu et al., 2025). The station data is pre-partitioned into a training set (130 stations), used for model  
90 development and validation, and a held-out test set (26 stations), used exclusively for final performance evaluation for all the three models selected in the study (Figure 1).

Topographic and geographic predictors are derived from a high-resolution DEM (Jarvis et al., 2008). These predictors serve as covariates in the RK model and as static input features for the DL models. We restricted our input predictors to those



95 derived from topographic data because the primary objective of this study is to identify an interpolation model configuration suitable for application to long-term daily climate time series (1901–present). For this extended historical period, dynamic covariates such as satellite products and land cover datasets are unavailable or inconsistent. Limiting the input to static, topographically derived predictors ensures temporal consistency and model applicability across the full time span.



100 **Figure 1 Spatial distribution of training and testing weather stations.**

## 2.2 Spatio-temporal covariates

A set of predictor variables was engineered to capture the primary drivers of spatial and temporal climate variability. These are grouped into static spatial predictors and dynamic temporal predictors.

105 Derived directly from the DEM for every station and grid point location, spatial predictors include smoothed elevation (*smooth\_elev*), a topographic position index (*topo\_position*), distance to the Black Sea (*dist\_to\_coast*), and geographic coordinates (*latwgs*, *lonwgs*) (Figure 2) (Daly et al., 2008). Calculated for each day to capture seasonal and long-term patterns, temporal predictors represent cyclical patterns without discontinuities, the day of the year and the month are transformed into sine and cosine components (*day\_sin*, *day\_cos*, *month\_sin*, *month\_cos*). A *year\_scaled* variable, representing the year linearly scaled to the [0, 1] range over the analysis period, is included to account for inter-annual trends.

110

These predictors are concatenated to form a feature vector for each observation point (*context*) and prediction grid point (*target*).

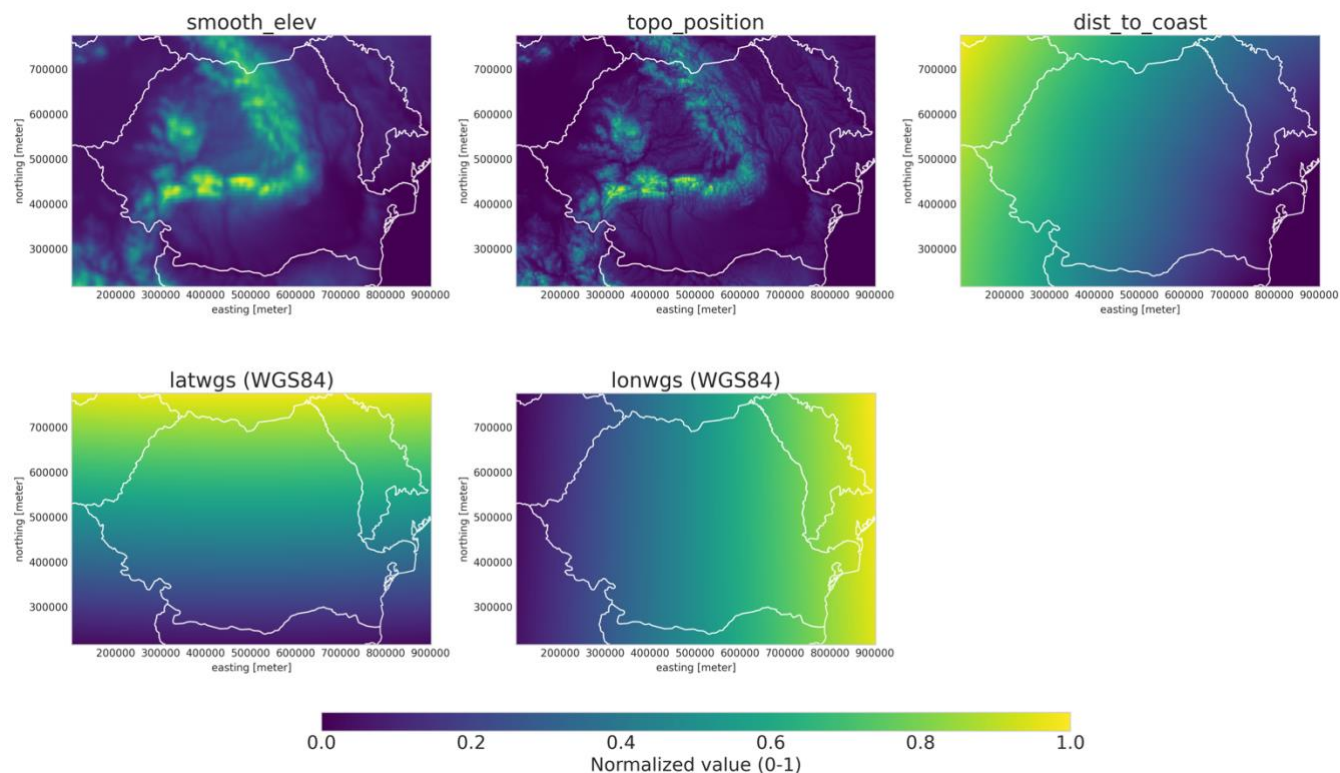


**Figure 2** Static predictors derived from DEM.

## 115 2.3 Data preprocessing

The raw data is processed into a format suitable for training the deep learning models. This involves normalization of the target variables and structuring the data into daily context and target sets.

The two climate variables, temperature and precipitation, are normalized independently. The daily mean temperature (*tavg*) is linearly scaled to a [0, 1] range using a *Min-Max scaler* fitted on the training data (Pedregosa et al., 2011). Raw precipitation (*prec*) values  $p$  are transformed via  $\log(1 + p)$  to handle zero values and reduce skewness, and the transformed values are then scaled to a [0, 1].

The parameters of these scalers are saved and used to de-normalize the model's predictions back to their original physical units ( $^{\circ}\text{C}$  and mm) during validation and inference.

## 3 Methods

125 The core of our study is the comparison of a standard approach — the geostatistical method Regression Kriging (RK) — with deep learning architectures, namely the Spatial Multi-Attention Conditional Neural Process (SMACNP). Unlike RK, the deep learning models are used to jointly predict both air temperature and precipitation in a single realisation. The



modelling approach differs fundamentally for the two variables due to their distinct statistical characteristics: air temperature, a continuous variable, is modelled directly, whereas daily precipitation, which is intermittent and non-negative, is handled using a two-part hurdle modelling framework in all tested configurations.

### 3.1 Regression Kriging (RK)

For air temperature, RK is applied directly to observed values. For precipitation, we employ a hurdle framework where occurrence and amount are modelled independently. The temperature and precipitation components are modelled as the sum of a deterministic trend, estimated via linear regression on topographic predictors, and a stochastic residual interpolated using Ordinary Kriging. As this is a well-established methodology, the detailed mathematical derivations for both variables are provided in Appendix A.

### 3.2 SMACNP

The SMACNP is a probabilistic deep learning model designed for interpolating sparse and irregularly distributed spatio-temporal data, and employs an encoder-decoder architecture.

The model is conditioned on a set of  $n$  context points representing observed data. Each context point consists of spatial coordinates ( $\mathbf{s}_c$ ), a vector of auxiliary attributes ( $\mathbf{a}_c$ ), and the corresponding climate variable measurement ( $\mathbf{y}_c$ ). Predictions are made at a set of  $m$  target locations, each defined by its spatial coordinates ( $\mathbf{s}_t$ ) and attributes ( $\mathbf{a}_t$ ) (Figure 3).

The encoder is composed of three parallel pathways that process the input data to generate a set of latent representations:

(1) Mean Location Encoder (Spatial Pathway) — This pathway is shared across all encoder configurations. It takes the concatenation of context spatial coordinates and observations  $[\mathbf{s}_c, \mathbf{y}_c]$  as input. The pathway first projects this input through an MLP and then applies Laplace Attention, which computes distance-based weights ( $\alpha_{ij}$ ) using a configurable  $L_p$  norm:

$$\alpha_{ij} = \frac{\exp\left(-\frac{\|\mathbf{s}_t^i - \mathbf{s}_c^j\|_p}{\tau}\right)}{\sum_{k=1}^n \exp\left(-\frac{\|\mathbf{s}_t^i - \mathbf{s}_c^k\|_p}{\tau}\right)} \quad (1)$$

where  $\tau$  is a learnable temperature parameter and  $p \in \{1,2\}$  selects between L1 (Manhattan) or L2 (Euclidean) distance. This produces a location-based representation  $\mathbf{w}^*$  that captures the spatial structure of the data.

(2) Mean Attribute Encoder (Attribute Pathway) — This pathway processes context information to produce an attribute-based representation  $\mathbf{r}^*$ . It projects the inputs into query ( $Q$ ), key ( $K$ ), and value ( $V$ ) vectors to compute a weighted representation using standard Multi-Head Attention. For a single head, the operation is defined as:



$$\text{Attention}(Q, K, V) = \text{softmax}\left(\frac{QK^T}{\sqrt{d_k}}\right)V \quad (2)$$

155 where  $d_k$  is the dimension of the keys. The distinction between the two configurations lies in the definition of the input sets used to construct these vectors:

160 • *Global Configuration*: The query  $Q$  is derived from target attributes  $\mathbf{a}_t$ . Keys  $K$  are derived from context attributes  $\mathbf{a}_c$  only (excluding observations), while values  $V$  are derived from both context attributes and observations  $[\mathbf{a}_c, \mathbf{y}_c]$ . This separation ensures that attention weights are computed purely based on attribute similarity, while the retrieved values incorporate the observed climate measurements. The mechanism computes attention over all context points, producing a full  $n \times m$  attention matrix. Spatial coordinates are intentionally excluded from this pathway, as spatial information is captured separately by the location encoder.

165 • *Localized Configuration*: The query  $Q$  incorporates target spatial and attribute features  $[\mathbf{s}_t, \mathbf{a}_t]$  (with optional positional encoding). Crucially, keys  $K$  are derived from context spatial and attribute features  $[\mathbf{s}_c, \mathbf{a}_c]$ , while values  $V$  additionally include observations  $[\mathbf{s}_c, \mathbf{a}_c, \mathbf{y}_c]$ . Both  $K$  and  $V$  are restricted to the  $k$  nearest spatial neighbors in the context set. This restricts attention to a local neighborhood  $k$ , reducing computational complexity from  $\mathcal{O}(nm)$  to  $\mathcal{O}(mk)$ . This localized attention mechanism introduces a strong inductive bias towards spatial locality, a critical feature for meteorological interpolation that has not been previously explored within the SMACNP framework for real-world climate data.

170 (3) Variance Encoder (Variance Pathway) — This pathway produces a representation  $\mathbf{v}^*$  for estimating predictive uncertainty. Crucially, observations ( $\mathbf{y}_c$ ) are excluded from the value ( $V$ ) in this pathway in both configurations to enable proper predictive uncertainty estimation without memorizing input-output relationships:

• *Global Configuration*: Takes context attributes only  $[\mathbf{a}_c]$  to form  $K$  and  $V$ , and target attributes  $[\mathbf{a}_t]$  for  $Q$ , using full  $n \times m$  multi-head cross-attention.

175 • *Localized Configuration*: Takes context spatial coordinates and attributes  $[\mathbf{s}_c, \mathbf{a}_c]$  (with optional positional encoding) to form  $K$  and  $V$ , and target features  $[\mathbf{s}_t, \mathbf{a}_t]$  for  $Q$ , using  $k$ -nearest neighbor attention.

The latent representations are routed to specialized decoder heads to generate the parameters for the predictive distributions. The location and attribute representations ( $\mathbf{w}^*, \mathbf{r}^*$ ) are concatenated with target point information ( $\mathbf{s}_t, \mathbf{a}_t$ ) and fed to the heads predicting mean values and probabilities. The variance representation ( $\mathbf{v}^*$ ) is similarly combined with target information and fed to the heads predicting variance. Each decoder head is implemented as an MLP.

180 In our implementation, the decoder is equipped with two specialized sets of output heads corresponding to the target variables:

(1) Temperature outputs — The temperature head parameterizes a Gaussian distribution through its mean ( $\mu$ ) and variance ( $\sigma^2$ ):

$$185 \quad p(y_t | \phi_t) = \mathcal{N}(y_t; \mu_t, \sigma_t^2) \quad (3)$$



The mean decoder uses a linear output activation (allowing negative temperatures), while the variance decoder applies a Softplus activation to ensure  $\sigma^2 > 0$ .

(2) Precipitation outputs — The precipitation head employs a hurdle model to handle the mixed discrete-continuous nature of precipitation data. The model produces three outputs: the probability of occurrence ( $p$ ), and the mean ( $\mu$ ) and variance ( $\sigma^2$ ) of the precipitation amount conditional on precipitation being nonzero. The decoder implements this through two distinct components:

a) Occurrence Model (Bernoulli): Models the probability of precipitation occurrence:

$$p(y_t > 0 | \phi_t^{\text{prob}}) = \text{Bernoulli}(p_t) \quad (4)$$

b) Amount Model (Log-Normal): Models the precipitation amount conditional on occurrence:

$$p(y_t | y_t > 0, \phi_t^{\text{amount}}) = \text{LogNormal}(\mu_t, \sigma_t^2) \quad (5)$$

The probability head outputs logits that are passed through a sigmoid function, while the mean and variance heads use *Softplus* activations to ensure positive outputs.

The model is trained end-to-end by minimizing the negative log-likelihood of the observed data. The total loss is a weighted combination of the temperature and precipitation losses:

$$\mathcal{L}_{\text{total}}(\theta) = w_{\text{temp}} \mathcal{L}_{\text{temp}}(\theta) + w_{\text{precip}} \mathcal{L}_{\text{precip}}(\theta) \quad (6)$$

(1) Temperature Loss — The standard Gaussian negative log-likelihood:

$$\mathcal{L}_{\text{temp}}(\theta) = \sum_{t \in T} \left[ \frac{1}{2} \log(2\pi\sigma_t^2) + \frac{(y_t - \mu_t)^2}{2\sigma_t^2} \right] \quad (7)$$

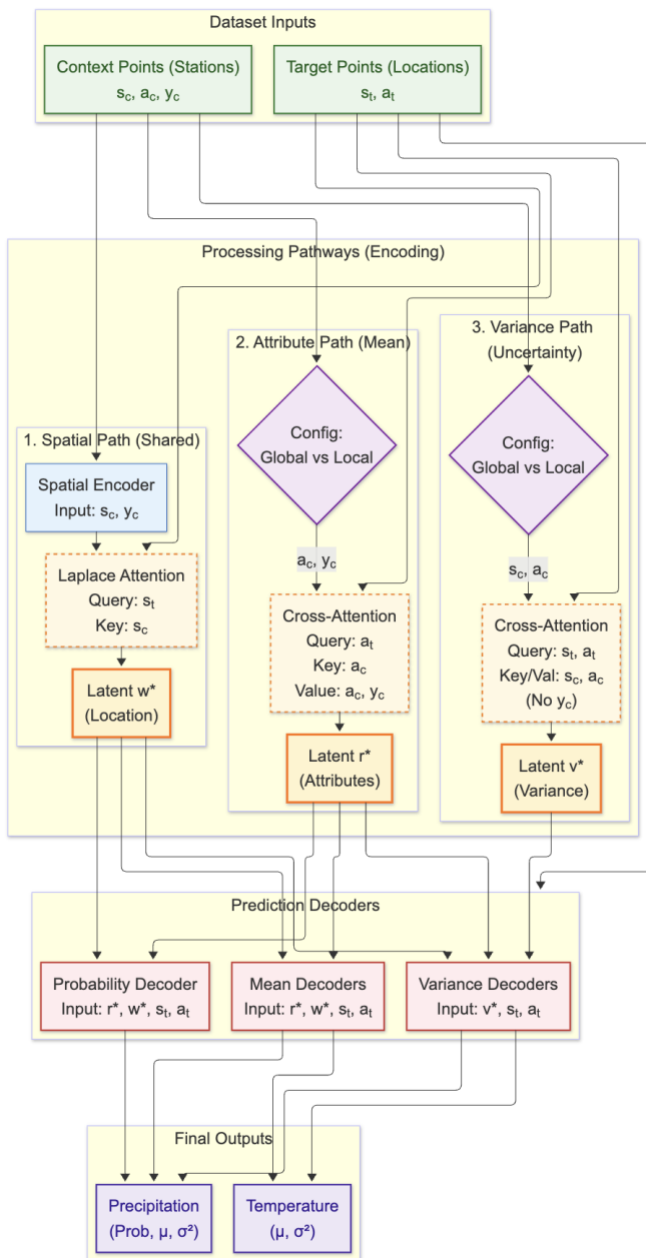
(2) Precipitation Loss — A weighted sum of the binary cross-entropy for the occurrence model and the negative log-likelihood of the Log-Normal distribution for the amount model:

$$\mathcal{L}_{\text{precip}}(\theta) = \sum_{t \in T} \left[ w_{\text{prob}} \cdot \text{BCE}(p_t, \mathbb{I}(y_t > 0)) + w_{\text{amount}} \cdot \mathbb{I}(y_t > 0) \cdot \text{NLL}_{\text{LogNorm}}(y_t; \mu_t, \sigma_t^2) \right] \quad (8)$$

where  $\mathbb{I}(y_t > 0)$  is an indicator function that equals 1 if precipitation is greater than zero and 0 otherwise, BCE denotes binary cross-entropy, and  $w_{\text{prob}}$ ,  $w_{\text{amount}}$  are weights balancing the two components.

To address class imbalance between rainy and dry days, the binary cross-entropy loss incorporates a positive class weight computed as the ratio of dry to rainy samples, capped at a maximum value to prevent instability:

$$w_{\text{pos}} = \min \left( \frac{n_{\text{dry}}}{n_{\text{rainy}}}, w_{\text{max}} \right) \quad (9)$$



215

**Figure 3** SMACNP architecture with dual encoder configurations. Three encoding pathways produce latent representations: spatial ( $w^*$ ) via Laplace attention, mean attributes ( $r^*$ ), and variance ( $v^*$ ). The mean and variance pathways offer interchangeable configurations: Global — full  $N \times M$  attention on attributes only; Localized —  $k$ -NN attention on spatial coordinates plus attributes with optional positional encoding. Note that the variance pathway excludes observations ( $y_c$ ) in both configurations to enable proper uncertainty estimation. Shared MLP decoders output temperature ( $\mu, \sigma^2$ ) and precipitation (probability  $p, \mu, \sigma^2$ ) predictions.



### 3.2 Experimental setup

An extensive hyperparameter optimization (HPO) was conducted for the SMACNP model for both *global* and *localized* encoder configurations to identify the optimal architecture and training settings. The HPO process was managed using the Optuna framework (Akiba et al., 2019). For each model variant, we executed a total of 1000 trials. The optimization was guided by a Tree-structured Parzen Estimator (TPE) sampler, initialized with a fixed random seed to ensure reproducibility. The objective for each trial was to minimize the model's validation loss. While the learning rate was included in the hyperparameter search space (ranging from  $1e-5$  to  $5e-4$ ), other training parameters were held constant. We used the *AdamW* optimizer with a weight decay of  $1e-5$ . The learning rate was managed by a scheduler configured to reduce the rate upon plateauing validation loss. To efficiently explore the search space, we implemented an aggressive early-stopping strategy, training each trial for up to 1,500 epochs. A patient pruner (wrapping a median pruner) was configured to terminate unpromising trials. Trials were pruned if their validation loss exceeded the median of previously completed trials for consecutive checks (patience of 5 checks), performed every 10 epochs after an initial warmup period (150 epochs).

The search spaces for the two configurations, including embedding dimensions, attention heads, and learning rates, are detailed in Appendix B. A constraint was enforced to ensure that embedding dimensions ( $r\_dim$ ,  $v\_dim$ ) were divisible by the number of attention heads.

Following the optimization process, the configurations yielding the lowest validation loss were selected for the final training and evaluation (Table B1). The SMACNP (Global) configuration favored a balanced architecture with a representation dimension ( $r\_dim$ ) of 128 and a variance dimension ( $v\_dim$ ) of 256. It utilized a shallower decoder (2 MLP layers) and higher attention complexity (16 heads) with minimal regularization (dropout rate of 0.1 and no layer normalization).

The SMACNP (Localized) configuration achieved optimal performance with a neighborhood size ( $k$ ) of 15 and, like the global variant, utilized the Manhattan distance metric ( $p = 1.0$ ) for the Laplace attention. This architecture optimized towards a highly asymmetric embedding structure, allocating significant capacity to the variance ( $v\_dim = 512$ ) and location ( $w\_dim = 256$ ) pathways relative to a compact representation dimension ( $r\_dim = 64$ ). While it favored a deeper decoder structure (3 MLP layers), the optimization process ultimately selected the same lightweight regularization settings as the global model—a dropout rate of 0.1 and no Layer Normalization—suggesting that the architectural bias of the localized encoder provided sufficient regularization without requiring heavy stochastic noise or normalization. Both models converged to similar learning rates, with the global variant at  $4.93 \times 10^{-4}$  and the localized variant at  $4.19 \times 10^{-4}$ .

## Results

We evaluated the results both qualitatively, by plotting multiannual-mean maps to verify that the predictions follow the expected spatial distribution of the analysed variables, and quantitatively, by computing accuracy metrics and corresponding plots using independent station data withheld from the training and prediction processes.



Visually, the outputs for air temperature from the three models are remarkably consistent (Figure 4 a), showing nearly identical spatial distributions, successfully capturing the expected climatological patterns driven by the topography. All methods correctly identify the same locations for the coldest areas in the mountain ranges and the warmest areas in the lowlands, displaying comparable temperature gradients. This suggests that the deep learning models are fully capable of reproducing the dominant geographical factors influencing temperature distribution as effectively as the geostatistical baseline. Similar to the temperature results, all three models successfully represent the fundamental influence of topography on precipitation (Figure 4 b). However, the visual differences in spatial detail are much more pronounced here. The RK model produces a slightly smoothed and generalized map; while it correctly identifies the broad zones of high precipitation in the Carpathians, the gradients are overly gradual, lacking fine-scale variability. In contrast, both SMACNP configurations generate significantly more detailed and textured precipitation fields. They resolve specific, concentrated areas of intense precipitation along mountain ridges and exhibit sharper transitions between wet and dry zones. These outputs appear physically more realistic, capturing the high spatial variability typical of precipitation in complex terrain, which the smoother RK baseline fails to resolve.

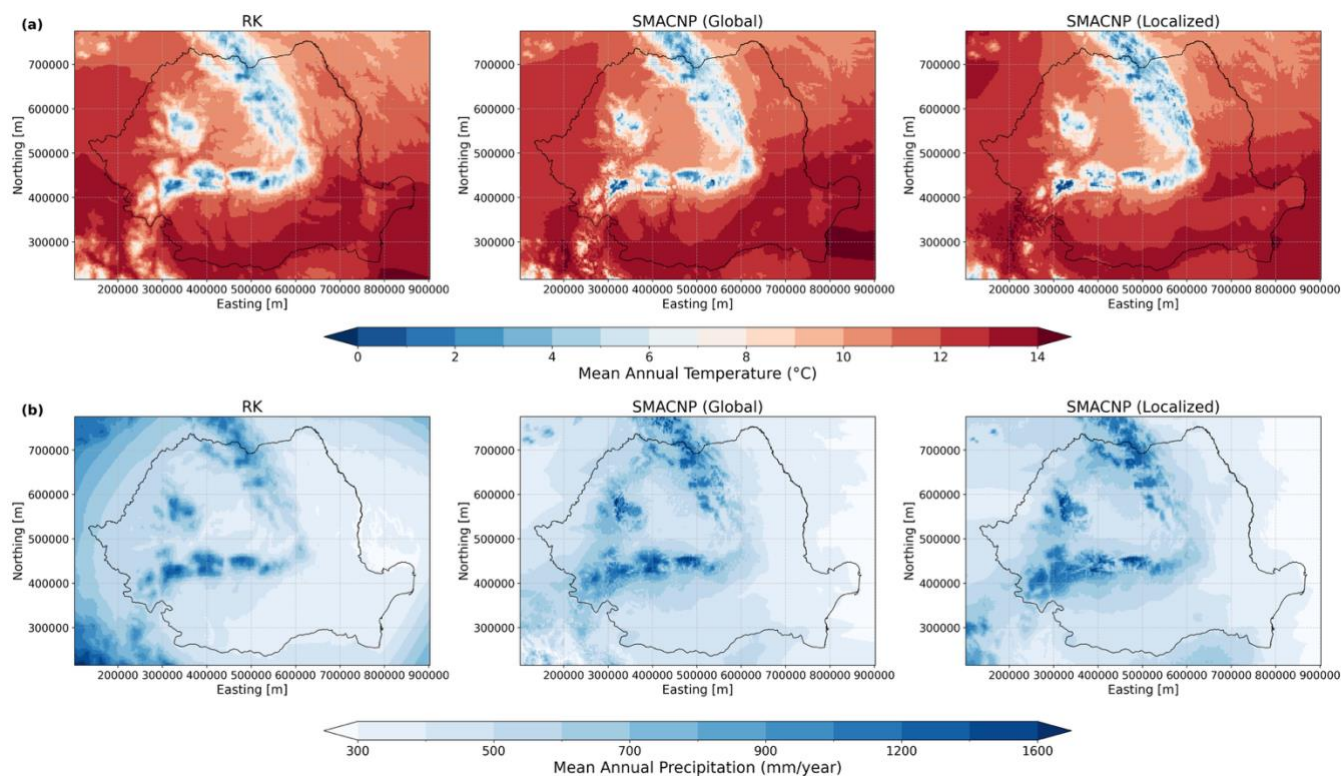


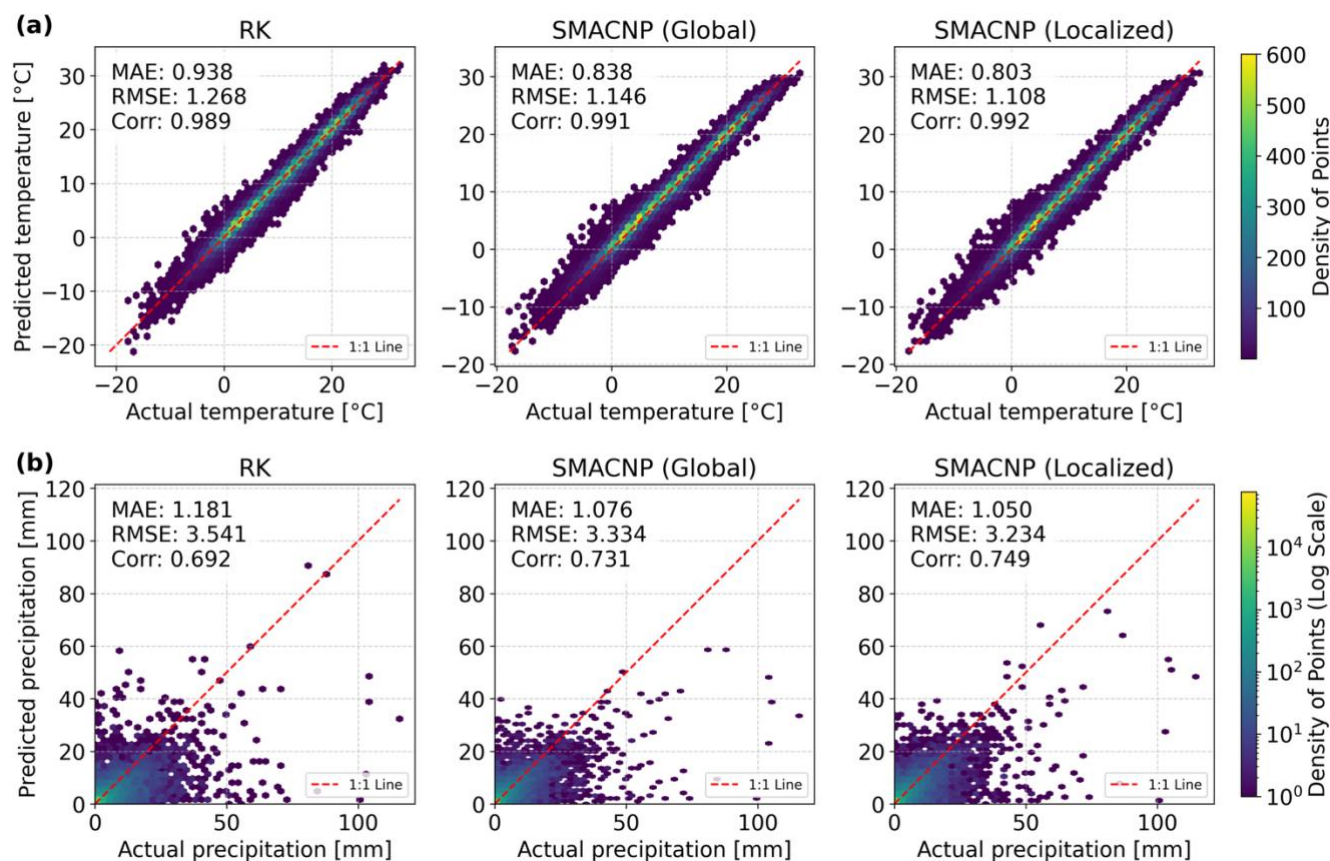
**Figure 4 Comparison of predicted mean annual temperature (a) and precipitation (b) from three models: RK, SMACNP (Global), and SMACNP (Localized).**

The density scatter plots in Figure 5 demonstrate that all three models provide highly accurate predictions for daily mean temperature (panel a), with points clustering tightly along the 1:1 line of perfect agreement. The RK baseline achieves a



correlation of 0.989 but exhibits slightly larger dispersion around the 1:1 line compared to the deep learning models, resulting in a higher MAE (0.938 °C). Both deep learning configurations outperform the baseline, with the SMACNP (Localized) variant achieving the best overall performance (MAE = 0.803 °C, RMSE = 1.108 °C), surpassing the SMACNP (Global) configuration (MAE = 0.838 °C). Across all models, prediction errors are slightly more pronounced in the tails of the distribution, yet the high density of points near the diagonal indicates strong agreement across the majority of the temperature range.

In contrast, the performance gap between the methods is more distinct for daily precipitation (panel b). Both SMACNP configurations substantially outperform the RK baseline, which suffers from larger errors (MAE = 1.181 mm) and a lower correlation (0.692). The SMACNP (Localized) model again delivers the strongest performance, achieving the lowest MAE (1.050 mm) and a correlation of 0.749, representing a notable improvement over the geostatistical baseline. While all models struggle with extreme precipitation events—a common challenge in climatological modeling—the deep learning approaches demonstrate a superior ability to capture the variability of moderate-to-high rainfall events compared to RK.



280

Figure 5 Density scatter plots of predicted versus actual (a) daily mean temperature (°C) and (b) daily precipitation (mm) for the three models on the test dataset: RK, SMACNP (Global), and SMACNP (Localized). For temperature, the colour of each



hexagonal bin indicates point density on a linear scale, while for precipitation (zero-inflated data), density is shown on a logarithmic scale. The dashed red line represents the 1:1 line of perfect agreement.

285 Across all seasons, SMACNP (Localized) and SMACNP (Global) consistently outperform the RK model for both  
 precipitation and temperature (Table 1). For temperature, all models perform well, with correlations exceeding 0.94 in all  
 cases. SMACNP (Localized) surpasses the others across all four seasons, consistently achieving the lowest MAE and RMSE,  
 reflecting its superior advantage in capturing fine-scale temperature variations compared to both the Global variant and the  
 RK baseline. For precipitation, SMACNP (Localized) demonstrates dominant performance, achieving the lowest MAE and  
 290 RMSE across all seasons, as well as the highest correlations (e.g., 0.808 in DJF). While SMACNP (Global) remains  
 competitive, SMACNP (Localized) outperforms it even in summer (JJA), yielding the lowest RMSE (4.958) and highest  
 correlation (0.677). The RK model exhibits the weakest performance, particularly for precipitation during JJA, where RMSE  
 reaches 5.374. Overall, the results demonstrate that neural process-based models substantially enhance predictive accuracy  
 over the baseline RK approach, especially for precipitation, where spatial heterogeneity and nonlinearity are more  
 295 pronounced. Based on its superior performance across the majority of metrics—particularly MAE—and seasons, SMACNP  
 (Localized) emerges as the most consistently high-performing method overall.

**Table 1 Seasonal evaluation metrics for temperature and precipitation across all models**

Season	Method	Temperature			Precipitation		
		MAE	RMSE	CORR	MAE	RMSE	CORR
<b>DJF</b>	RK	1.038	1.445	0.947	0.862	2.289	0.758
	SMACNP (Global)	0.950	1.327	0.957	0.796	2.205	0.780
	SMACNP (Localized)	<b>0.902</b>	<b>1.296</b>	<b>0.957</b>	<b>0.756</b>	<b>2.066</b>	<b>0.808</b>
<b>MAM</b>	RK	0.889	1.176	0.982	1.034	2.773	0.727
	SMACNP (Global)	0.798	1.060	0.984	0.915	2.509	0.783
	SMACNP (Localized)	<b>0.737</b>	<b>0.985</b>	<b>0.986</b>	<b>0.903</b>	<b>2.497</b>	<b>0.784</b>
<b>JJA</b>	RK	0.856	1.131	0.969	1.912	5.374	0.606
	SMACNP (Global)	0.742	0.987	0.972	1.769	5.100	0.655
	SMACNP (Localized)	<b>0.733</b>	<b>0.961</b>	<b>0.973</b>	<b>1.739</b>	<b>4.958</b>	<b>0.677</b>
<b>SON</b>	RK	0.973	1.301	0.978	0.907	2.859	0.787
	SMACNP (Global)	0.866	1.185	0.981	0.817	2.670	0.815
	SMACNP (Localized)	<b>0.845</b>	<b>1.160</b>	<b>0.982</b>	<b>0.793</b>	<b>2.570</b>	<b>0.830</b>

300

To complement the error analysis, we further examine how well the models quantify uncertainty and represent the full precipitation distribution (Figure 6 and



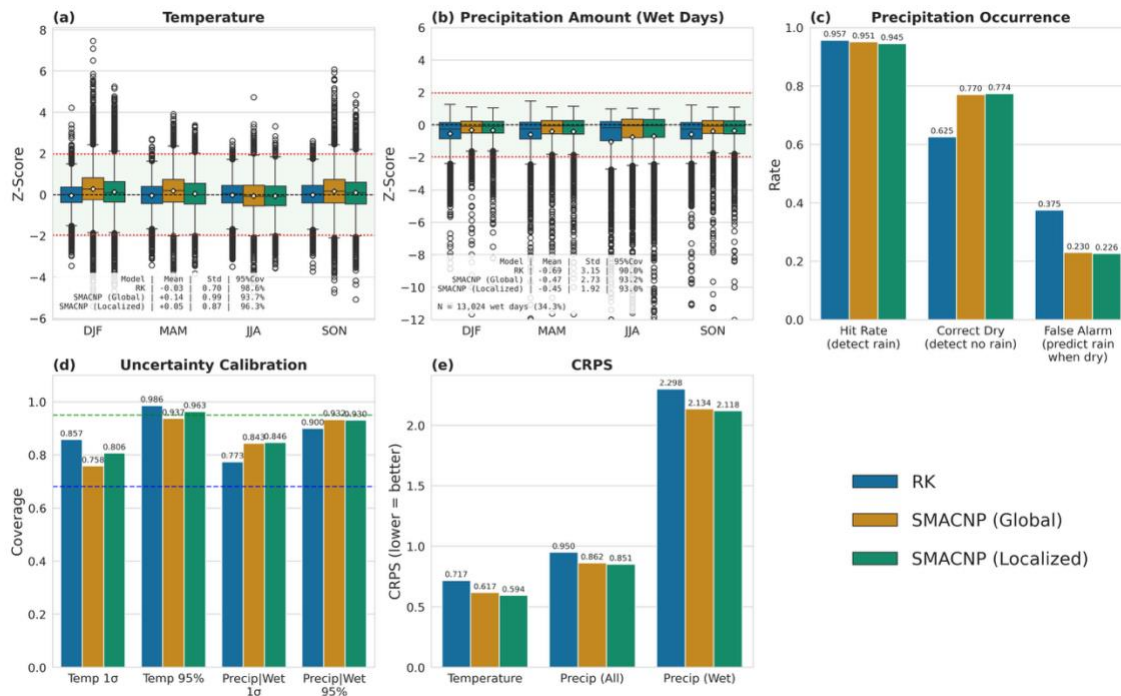
305

310 Table 2). For temperature (panel a), the z-score distributions show mean values generally close to zero (Table 2;  $|\text{mean } z| \leq$   
0.14), though SMACNP (Global) shows a slight positive bias (+0.14). The RK baseline exhibits a narrow z-score  
distribution (std  $\approx 0.70$ ) resulting in conservative, over-dispersive 95% intervals (95% coverage  $\approx 0.99$ ). SMACNP (Global)  
approaches a standard normal distribution (std  $\approx 0.99$ ) with slightly under-dispersive coverage (93.7%), while SMACNP  
(Localized) maintains a standard deviation of  $\approx 0.87$  and achieves coverage closest to nominal ( $1\sigma$ : 0.81, 95%: 0.96). These  
315 improvements are reflected in the temperature CRPS, where both SMACNP configurations outperform RK (0.59–0.62 vs  
0.72, with a slight advantage for the localized model). For precipitation amounts on wet days (panel b), all models exhibit  
negative mean z-scores, indicating a systematic underestimation of the intensity of rainy events. This bias is strongest for RK  
(mean  $z \approx -0.70$ ) and reduced for the SMACNP variants ( $\approx -0.46$  to  $-0.47$ ). The spread of z-scores is much larger than one  
for all models, reflecting the strong skewness and heavy tails of the wet-day distribution, but again the deep models show  
320 substantial gains: the standard deviation drops from  $\approx 3.15$  (RK) to 2.73 (SMACNP Global) and 1.92 (SMACNP Localized).  
The 95% coverage on wet days increases from 0.90 for RK to about 0.93 for both SMACNP variants, indicating that extreme  
wet events are captured more reliably, though some under-dispersion remains. Consistently, the CRPS for wet-day  
precipitation decreases from 2.30 (RK) to 2.13 and 2.12 for the global and localized SMACNP models, respectively. Panel  
(c) focuses on precipitation occurrence, implicitly derived from the marginal predictive distributions. All models maintain  
325 high hit rates for rainy days ( $\approx 0.95$ – $0.96$ ), but they differ notably in how often they falsely predict rain. RK strongly  
overestimates the frequency of wet days (predicted wet fraction  $\approx 0.57$  vs observed  $\approx 0.34$ ), leading to a high false-alarm rate  
of about 0.38 and a relatively low correct-dry rate of 0.63. Both SMACNP configurations bring the predicted wet fraction  
much closer to the observed value ( $\approx 0.47$ – $0.48$ ), reduce the false-alarm rate to about 0.23, and increase the correct-dry rate  
to  $\approx 0.77$ . This indicates fewer spurious light-rain estimates while preserving sensitivity to true rain events. The coverage  
330 summary in panel (d) integrates these results. For temperature, RK over-covers at the 95% level (0.99), whereas SMACNP  
(Global) slightly under-covers (0.94) and SMACNP (Localized) is near-ideal (0.96). For wet-day precipitation, the RK  
intervals are too narrow in the tails (95% coverage  $\approx 0.90$ ), while SMACNP models increase the 95% coverage to  $\approx 0.93$  and  
modestly over-cover at  $1\sigma$  (0.84), consistent with somewhat wider but more reliable uncertainty intervals. Finally, the CRPS  
scores in panel (e) summarise overall probabilistic skill in a distribution-agnostic way. For both temperature and  
335 precipitation (all days and wet days only), the two SMACNP variants consistently achieve lower CRPS than RK, with the



340

localized version marginally outperforming the global one. Taken together, these diagnostics show that the deep learning approaches, and particularly SMACNP (Localized), not only reduce deterministic errors but also provide better-calibrated and more informative uncertainty estimates, especially for precipitation occurrence and intensity.



345 **Figure 6** Seasonal uncertainty calibration and overall probabilistic verification. (a) Seasonal distributions of standardized errors (z-scores) for temperature. (b) As in (a), but for precipitation amounts on wet days only (observed precipitation > 0.1 mm; sample size and wet-day fraction indicated in the panel). Z-scores are defined as (prediction – observation) / predicted\_std; the red horizontal lines mark ±1.96, corresponding to the 95% interval of a standard normal distribution and used as a visual reference for well-calibrated predictions (mean ≈ 0, std ≈ 1). (c) Precipitation occurrence scores implicitly derived from the marginal predictive distributions: hit rate for rain detection, correct-dry rate, and false-alarm rate (predicting rain when it is dry). (d) 350 Empirical coverage of the nominal 1σ and 95% predictive intervals for temperature and precipitation (wet days), with dashed horizontal lines indicating the expected values of 0.68 and 0.95. (e) Continuous Ranked Probability Score (CRPS) for temperature, all-day precipitation, and wet-day precipitation (lower values indicate better probabilistic skill).

355



360

365 **Table 2 Summary of probabilistic verification metrics for temperature and precipitation. Metrics are aggregated over all seasons**  
**and stations for the three methods (RK, SMACNP Global, SMACNP Localized). For temperature, CRPS quantifies overall**  
**probabilistic skill (lower is better), “95% Cov” is the empirical coverage of the nominal 95% predictive interval, and “Mean Z” is**  
**the mean standardized error, with an ideal value of 0. For precipitation detection, scores are computed using an occurrence**  
 370 **threshold of 0.1 mm: Hit Rate is the fraction of wet days correctly detected, FAR (false alarm rate) is the fraction of dry days on**  
**which rain is predicted, and True Dry is the fraction of dry days correctly forecast as dry. For precipitation intensity, CRPS, 95%**  
**coverage and Mean Z are evaluated on wet days only (observed precipitation > 0.1 mm). An ideal model has low CRPS and FAR,**  
**high Hit Rate and True Dry, 95% Cov close to 0.95, and |Mean Z| close to zero.**

Method	Temperature				Precipitation (Detection)			Precipitation (Intensity)			
	CRPS	95% Cov	Mean Z	Std Z	Hit Rate	FAR	True Dry	CRPS	95% Cov	Mean Z	Std Z
<b>RK</b>	0.717	0.986	<b>-0.031</b>	0.703	<b>0.957</b>	0.375	0.625	2.298	0.900	-0.695	3.152
<b>SMACNP</b> <b>(Global)</b>	0.617	0.937	0.136	<b>0.995</b>	0.951	0.230	0.770	2.134	<b>0.932</b>	-0.466	2.732
<b>SMACNP</b> <b>(Localized)</b>	<b>0.594</b>	<b>0.963</b>	0.050	0.874	0.945	<b>0.226</b>	<b>0.774</b>	<b>2.118</b>	0.930	<b>-0.455</b>	<b>1.916</b>

375 Figure 7 provides a time-series comparison of model performance for daily mean air temperature and total precipitation at  
 the Bacău station (174 m a.m.s.l.) throughout 2023, selected from the test data subset. The figure shows the ground truth  
 observations against the predictions from the three evaluated models.

For air temperature, all three models demonstrate a strong ability to capture the seasonal cycle and daily fluctuations, closely  
 tracking the ground truth data. The shaded areas, representing the 95% confidence intervals, are relatively narrow for all  
 380 models, indicating a high degree of certainty in their temperature predictions, though the RK intervals are noticeably wider  
 than those of the deep learning models. The MAE values inset in the plot show that the deep learning models outperform the  
 baseline, with SMACNP (Localized) achieving the lowest MAE of 0.468°C, followed by SMACNP (Global) at 0.488°C,  
 both improving upon the RK model's MAE of 0.575°C.



The lower panel, illustrating total precipitation, reveals the challenges in modeling this discontinuous variable. While all models capture the timing of major precipitation events, the SMACNP (Localized) model demonstrates the best performance in predicting the magnitude of these events, as evidenced by its lower MAE of 0.663 mm. SMACNP (Global) follows closely with an MAE of 0.687 mm, while the RK model has the highest MAE at 0.789 mm. The 95% confidence intervals are visibly wider for precipitation than for temperature across all models, reflecting the greater inherent uncertainty in predicting this variable. Notably, the confidence intervals for the deep learning models, particularly SMACNP (Localized), often envelop the observed precipitation peaks more effectively than the RK model, suggesting a more reliable quantification of uncertainty. This is especially apparent during the intense precipitation events observed in September and November. Corresponding time-series comparisons for all other stations in the test set are provided in the Supplement (Figures S1–S25), demonstrating consistent performance across diverse elevations and locations.

395

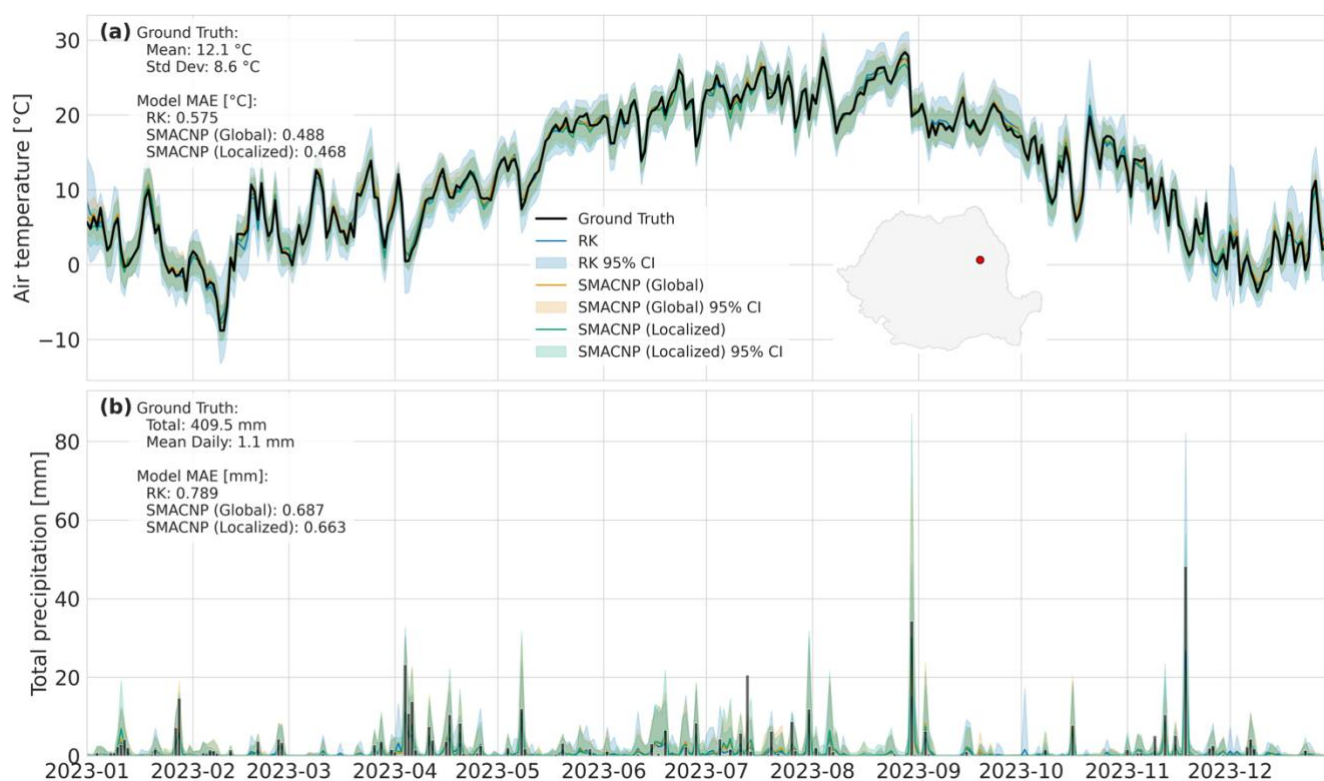


**Figure 7** Model performance and uncertainty at Bacău station (428 m a.m.s.l.). Time series comparison of (a) daily average temperature and (b) daily total precipitation for the year 2023. Shaded areas represent the 95% confidence interval for each model's prediction. The inset map shows the location of the station within the study area, marked by a red dot.



## 400 5 Discussions

The superior performance of the neural process models, particularly for precipitation, can be attributed to their ability to learn complex, non-linear relationships directly from the data. Unlike RK, which relies on a pre-defined linear model for the trend and a stationary variogram for the residuals, deep learning architectures can capture the intricate interplay between topography, location, and climate variables. This is especially critical for precipitation, whose spatial distribution in mountainous terrain is often intermittent, highly localized, and non-stationary—conditions that violate the core assumptions of RK and explain its tendency to produce overly smooth and generalized outputs.

Among the two deep learning architectures, the good results of the SMACNP with a *localized* encoder highlights the benefit of incorporating a strong structural prior into the model design. This approach aligns with the principles driving recent breakthroughs in global weather forecasting, where models like Google's GraphCast and ECMWF AIFS have demonstrated the importance of effectively capturing local spatial dependencies (Lam et al., 2023; Moldovan et al., 2025). In our application, by restricting the attention mechanism to a  $k - NN$ , the localized encoder is explicitly guided to learn representations based on spatial proximity. This provides a powerful inductive bias for modeling climate variables, contrasting with the more flexible, but less constrained, global attention mechanism of the standard SMACNP. Moreover, the localized configuration offers superior computational efficiency when generating high-resolution grids. By limiting interactions to the  $k$  nearest neighbors ( $k - NN$ ) rather than computing global pairwise correlations, it avoids the quadratic complexity of the global encoder, making it significantly more scalable for producing dense gridded outputs. Building on this, future studies could further enhance the configuration by incorporating explicit graph structures within the encoder. Adopting Graph Neural Network (GNN) architectures would allow for sophisticated message passing between observation points, potentially capturing complex, non-linear spatial dependencies more effectively than the current attention-based neighborhood aggregation.

The practical importance of well-calibrated uncertainty cannot be overstated. For applications such as flood risk assessment or agricultural modeling, an unbiased estimate of the prediction's confidence is as valuable as the prediction itself. Our analysis reveals that only SMACNP (Localized) provides reliable uncertainty estimates across both temperature and precipitation. The severe overconfidence of the RK model's precipitation uncertainties renders them impractical for risk-aware decision-making. Furthermore, the uncertainty quantification of the deep learning models could be enhanced by adopting a deep ensemble approach. As demonstrated in the creation of a global canopy height map from satellite imagery (Lang et al., 2023), training an ensemble of models with different random initializations offers a robust approach to estimate epistemic uncertainty—the model's lack of knowledge in regions or conditions underrepresented in the training data. The variation among ensemble predictions provides a direct measure of model confidence. While the inherent probabilistic design of our SMACNP (Localized) already captures aleatoric uncertainty, combining it with an ensemble strategy would yield a more comprehensive and reliable characterization of total predictive uncertainty, further supporting the adoption of such frameworks for operational climate datasets.



Remarkably, the SMACNP models achieved superior accuracy compared to the RK baseline, even though it was constrained to model temperature and precipitation simultaneously. While RK had the advantage of fitting distinct models for each  
435 variable, the deep learning approach demonstrated that a unified architecture could leverage shared spatio-temporal features to outperform the specialized, single-variable geostatistical models.

It is also pertinent to address the architectural selection for this study. During the initial phases, we evaluated other neural process variants, including the ConvCNP and GriddedTNP. However, these models failed to yield satisfactory results under the strict constraints of our experimental setup; the combination of a very sparse observation network (130 stations) and the  
440 exclusion of dynamic covariates appeared to hinder the ability of these architectures to resolve local features effectively. While GriddedTNP is designed to scale efficiently to large datasets, it likely struggled to construct a robust latent grid representation from such sparse inputs. The SMACNP architecture proved suited to this data-scarce regime because its attention mechanism explicitly models directly the relationship between specific context and target points based on topographic similarity, rather than relying on grid-based projections or convolutions that typically require denser data to  
445 perform optimally.

It is important to acknowledge the limitations of this study. Our analysis was intentionally restricted to static, topographically-derived predictors to ensure the developed models are applicable to long-term historical datasets where dynamic covariates like satellite imagery products are unavailable. The inclusion of dynamic predictors could further enhance model performance for modern periods.

## 450 **6 Conclusions**

In this study, we evaluated and compared a traditional geostatistical interpolation method, Regression Kriging (RK), with two advanced deep learning models, the Spatial Multi-Attention Conditional Neural Process (SMACNP) with Localized and Global encoders, for producing daily gridded fields of air temperature and precipitation from a very sparse station data in Romania.

455 The primary conclusions of this work are as follows:

1. Deep learning models substantially outperform the geostatistical baseline. Both SMACNP configurations demonstrated significantly higher accuracy than RK for both climate variables. The performance gains were particularly large for precipitation, where the neural process models were better able to capture the complex, non-linear, and heterogeneous spatial patterns inherent to rainfall in a topographically diverse region.
- 460 2. SMACNP (Localized) is the most robust and highest-performing model. Our study identifies this specific configuration as a novel and highly effective approach for sparse data interpolation. By explicitly leveraging local neighborhood structure via a localized encoder, the SMACNP (Localized) model consistently achieved the best or near-best performance across most evaluation metrics and seasons. It excelled at creating detailed and realistic spatial fields while minimizing prediction errors.



465 3. Probabilistic deep learning provides superior uncertainty quantification. A key advantage of the neural process  
framework is its native ability to provide probabilistic predictions. The SMACNP (Localized) model, in particular,  
produced well-calibrated and reliable uncertainty estimates for both temperature and precipitation. In contrast, the  
RK model's precipitation uncertainty estimates showed signs of overconfidence, reducing their reliability.

Our findings demonstrate that a unified deep learning framework can outperform specialized univariate geostatistical  
470 models, effectively leveraging shared spatio-temporal patterns to improve accuracy across multiple climate variables  
simultaneously. The ability of these models to learn from data to represent complex spatial dependencies, combined with  
their capacity for reliable uncertainty estimation, makes them exceptionally well-suited for the development of high-quality  
gridded climate datasets. The results of this study provide a strong methodological foundation for the future production of a  
new, long-term, high-resolution daily climate dataset.

475

## Appendix A Regression Kriging Formulation

The temperature  $Z$  at a location  $s$  is modeled as the sum of a deterministic trend  $m(s)$  and a stochastic, spatially correlated  
residual  $R(s)$ :

480 
$$Z(s) = m(s) + R(s) \quad (A1)$$

The prediction  $\hat{Z}(s_0)$  at a target location  $s_0$  is derived in three steps:

(1) The trend  $m(s)$  is estimated using a multiple linear regression model based on a set of  $p$  predictor variables  $x_k(s)$ .

The estimated trend  $\hat{m}(s)$  is:

485 
$$\hat{m}(s) = \hat{\beta}_0 + \sum_{k=1}^p \hat{\beta}_k x_k(s) \quad (A2)$$

where  $\hat{\beta}_k$  are the regression coefficients fitted using the data at the station locations.

(2) The residuals at the  $n$  station locations  $s_i$  are calculated as:

$$R(s_i) = Z(s_i) - \hat{m}(s_i) \quad (A3)$$

490 These residuals are then interpolated to the target location  $s_0$  using ordinary kriging (OK). The kriged residual  $\hat{R}(s_0)$  is a  
weighted average of the observed residuals:

$$\hat{R}(s_0) = \sum_{i=1}^n w_i(s_0) R(s_i) \quad (A4)$$

where the weights  $w_i$  are determined by solving the kriging equations based on a fitted spherical variogram model of the  
residuals.



(3) The final temperature prediction is the sum of the estimated trend and the kriged residual:

495

$$\hat{Z}(s_0) = \hat{m}(s_0) + \hat{R}(s_0) \quad (A5)$$

A hurdle model is used for precipitation  $Y(s)$ , which separates the process into two parts: the probability of rain and the amount of rain if it occurs. The final prediction  $\hat{Y}(s_0)$  is the statistical expectation:

$$\hat{Y}(s_0) = P(Y(s_0) > 0) \cdot E[Y(s_0)|Y(s_0) > 0] \quad (A6)$$

Probability of precipitation  $P(Y(s_0) > 0)$  is estimated using a logistic regression model. The probability  $p(s)$  at a location  $s$  is modeled as:

500

$$\text{logit}(p(s)) = \log\left(\frac{p(s)}{1-p(s)}\right) = \gamma_0 + \sum_{k=1}^p \gamma_k x_k(s) \quad (A7)$$

The predicted probability  $\hat{p}(s_0)$  at the target location is the output of this model. The amount of precipitation, conditioned on rain occurring  $E[Y(s_0)|Y(s_0) > 0]$ , is modeled using RK on log-transformed data for rainy stations only  $L(s) = \log(Y(s) + 1)$ . The process mirrors the RK model for temperature:

505

(1) A linear model is fitted for  $L(s)$  at rainy stations:

$$\hat{m}_L(s) = \hat{\alpha}_0 + \sum_{k=1}^p \hat{\alpha}_k x_k(s) \quad (A8)$$

(2) Residuals  $R_L(s_i) = L(s_i) - \hat{m}_L(s_i)$  are computed and kriged to get  $\hat{R}_L(s_0)$

(3) Prediction (Log-scale):

$$\hat{L}(s_0) = \hat{m}_L(s_0) + \hat{R}_L(s_0) \quad (A9)$$

510 The predicted amount is obtained by back-transforming the result:  $\exp(\hat{L}(s_0)) - 1$

(4) The final precipitation prediction is the product of the two parts:

$$\hat{Y}(s_0) = \hat{p}(s_0) \cdot (\exp(\hat{L}(s_0)) - 1) \quad (A10)$$

## Appendix B Hyperparameter Optimization Details

SMACNP (Global Encoder):

515

- Embedding Dimensions (r\_dim, v\_dim): categorical [64, 128, 256, 512]
- Location Encoder Dimension (w\_dim): categorical [64, 128, 256, 512]
- Hidden Size: categorical [256, 512, 1024]
- Attention Heads: categorical [4, 8, 16]
- MLP Layers: categorical [2, 3]

520

- Dropout Rate: float [0.1, 0.3] with a step of 0.05
- Laplace Distance ( $p$ ): categorical [1.0, 2.0]



- Learning Rate: float [1e-4, 5e-4] (log scale)

SMACNP (Localized Encoder):

- 525
- Embedding Dimensions ( $r\_dim$ ,  $v\_dim$ ): categorical [64, 128, 256, 512]
  - Location Encoder Dimension ( $w\_dim$ ): categorical [64, 128, 256, 512]
  - Hidden Size: categorical [256, 512, 1024]
  - Attention Heads: categorical [4, 8, 16]
  - MLP Layers: categorical [2, 3]
- 530
- Dropout Rate: float [0.1, 0.3] with a step of 0.05
  - Localized Neighbors ( $k$ ): categorical [15, 20, 25, 30]
  - Laplace Distance ( $p$ ): categorical [1.0, 2.0]
  - Learning Rate: float [1e-4, 5e-4] (log scale)

535

**Table B1 Optimal hyperparameters selected via TPE optimization for the Global and Localized SMACNP configurations.**

Hyperparameter	SMACNP (Global)	SMACNP (Localized)
<b>Embedding Dimensions</b>		
Representation ( $r\_dim$ )	128	64
Location ( $w\_dim$ )	64	256
Variance ( $v\_dim$ )	256	512
Hidden Size	512	512
<b>Architecture</b>		
Attention Heads	16	8
MLP Layers	2	3
<b>Regularization &amp; Training</b>		
Dropout Rate	0.1	0.1
Layer Normalization	False	False
Learning Rate	$4.93 \times 10^{-4}$	$4.19 \times 10^{-4}$
<b>Encoder-Specific</b>		
Neighbors ( $k$ )	N/A	15
Distance ( $p$ )	1.0 (Manhattan)	1.0 (Manhattan)



### **Code and data availability**

The source code developed for this study (SMACNP architectures: Global and Localized; Regression Kriging baseline; and  
540 training scripts) is publicly available on GitHub and archived on Zenodo: <https://github.com/alex dum/ climate-gridder>;  
<https://doi.org/10.5281/zenodo.18763498> (Dumitrescu, 2026). The homogenized daily air temperature and precipitation  
dataset (2020–2023) used for model development and evaluation, together with station metadata, is openly available via  
Zenodo at <https://zenodo.org/records/14880417> (Dumitrescu, 2025).

### **Supplement link**

545 The link to the supplement will be included by Copernicus, if applicable.

### **Author contributions**

AD is responsible for all aspects of this work, including conceptualization, methodology, software, validation, formal  
analysis, data curation, and writing – original draft preparation.

### **Competing interests**

550 The author declares that there is no conflict of interest.

### **Disclaimer**

Copernicus Publications adds a standard disclaimer: “Copernicus Publications remains neutral with regard to jurisdictional  
claims made in the text, published maps, institutional affiliations, or any other geographical representation in this paper.  
While Copernicus Publications makes every effort to include appropriate place names, the final responsibility lies with the  
555 authors. Views expressed in the text are those of the authors and do not necessarily reflect the views of the publisher.”  
Please feel free to add disclaimer text at your choice, if applicable.

### **Acknowledgements**

This research was supported by the project “Cross-sectoral Framework for Socio-Economic Resilience to Climate Change  
and Extreme Events in Europe (CROSSEU)” funded by the European Union Horizon Europe Programme, under Grant  
560 agreement n° 101081377.



The author used Grammarly to refine the phrasing and correct grammatical errors in the text. The author reviewed and takes full responsibility for the final content.

### Financial support

This research has been supported by the European Union Horizon Europe Programme, under Grant agreement n°  
565 101081377.

### Review statement

The review statement will be added by Copernicus Publications listing the handling editor as well as all contributing referees according to their status anonymous or identified.

### 570 References

- Akiba, T., Sano, S., Yanase, T., Ohta, T., and Koyama, M.: Optuna: A Next-generation Hyperparameter Optimization Framework, in: Proceedings of the 25th ACM SIGKDD International Conference on Knowledge Discovery and Data Mining, 2019.
- Appelhans, T., Mwangomo, E., Hardy, D. R., Hemp, A., and Nauss, T.: Evaluating machine learning approaches for the  
575 interpolation of monthly air temperature at Mt. Kilimanjaro, Tanzania, *Spat. Stat.*, 14, 91–113, <https://doi.org/10.1016/j.spasta.2015.05.008>, 2015.
- Ashman, M., Diaconu, C., Langezaal, E., Weller, A., and Turner, R. E.: Gridded Transformer Neural Processes for Large Unstructured Spatio-Temporal Data, <https://doi.org/10.48550/arXiv.2410.06731>, 10 October 2024.
- Bao, L.-L., Zhang, C.-X., Zhang, J.-S., and Guo, R.: A two-stage spatial prediction modeling approach based on graph neural  
580 networks and neural processes, *Expert Syst. Appl.*, 258, 125173, <https://doi.org/10.1016/j.eswa.2024.125173>, 2024a.
- Bao, L.-L., Zhang, J.-S., and Zhang, C.-X.: Spatial multi-attention conditional neural processes, *Neural Netw.*, 173, 106201, <https://doi.org/10.1016/j.neunet.2024.106201>, 2024b.
- Carr, A. and Wingate, D.: Graph Neural Processes: Towards Bayesian Graph Neural Networks, <https://doi.org/10.48550/arXiv.1902.10042>, 1 October 2019.
- 585 Daly, C., Neilson, R. P., and Phillips, D. L.: A Statistical-Topographic Model for Mapping Climatological Precipitation over Mountainous Terrain, *J. Appl. Meteorol.*, 33, 140–158, [https://doi.org/10.1175/1520-0450\(1994\)033%253C0140:ASTMFM%253E2.0.CO;2](https://doi.org/10.1175/1520-0450(1994)033%253C0140:ASTMFM%253E2.0.CO;2), 1994.



- Daly, C., Halbleib, M., Smith, J. I., Gibson, W. P., Doggett, M. K., Taylor, G. H., Curtis, J., and Pasteris, P. P.: Physiographically sensitive mapping of climatological temperature and precipitation across the conterminous United States, 590 *Int. J. Climatol.*, 28, 2031–2064, <https://doi.org/10.1002/joc.1688>, 2008.
- Diggle, P. J. and Ribeiro, P. J.: *Model-based Geostatistics*, Springer New York, New York, NY, <https://doi.org/10.1007/978-0-387-48536-2>, 2007.
- Dosovitskiy, A., Beyer, L., Kolesnikov, A., Weissenborn, D., Zhai, X., Unterthiner, T., Dehghani, M., Minderer, M., Heigold, G., Gelly, S., Uszkoreit, J., and Houlsby, N.: An Image is Worth 16x16 Words: Transformers for Image 595 Recognition at Scale, <https://doi.org/10.48550/ARXIV.2010.11929>, 2020.
- Dumitrescu, A.: RoCliHom - Long-term homogenized air temperature and precipitation datasets in Romania, 1901 - 2023 (1.0.0), <https://doi.org/10.5281/ZENODO.14880417>, 2025.
- Dumitrescu, A.: Climate Gridder: SMACNP and Regression Kriging for Climate Field Construction, , <https://doi.org/10.5281/ZENODO.18763498>, 2026.
- 600 Dumitrescu, A., Micu, D., Guijarro, J., Manea, A., and Cheval, S.: Long-term homogenized air temperature and precipitation datasets in Romania, 1901–2023, *Sci. Data*, 12, 1116, <https://doi.org/10.1038/s41597-025-05371-4>, 2025.
- Garnelo, M., Rosenbaum, D., Maddison, C., Ramalho, T., Saxton, D., Shanahan, M., Teh, Y. W., Rezende, D., and Eslami, S. A.: Conditional neural processes, in: *International conference on machine learning*, 1704–1713, 2018.
- Gordon, J., Bruinsma, W. P., Foong, A. Y. K., Requeima, J., Dubois, Y., and Turner, R. E.: Convolutional Conditional 605 Neural Processes, <https://doi.org/10.48550/ARXIV.1910.13556>, 2019.
- Hengl, T., Heuvelink, G. B., and Rossiter, D. G.: About regression-kriging: from equations to case studies, *Comput. Geosci.*, 33, 1301–1315, 2007.
- Hijmans, R. J., Cameron, S. E., Parra, J. L., Jones, P. G., and Jarvis, A.: Very high resolution interpolated climate surfaces for global land areas, *Int. J. Climatol.*, 25, 1965–1978, <https://doi.org/10.1002/joc.1276>, 2005.
- 610 Iwase, K. and Takenawa, T.: Interpolation of mountain weather forecasts by machine learning, <https://doi.org/10.48550/arXiv.2308.13983>, 14 August 2024.
- Jarvis, A., Reuter, H. I., Nelson, A., and Guevara, E.: Hole-filled seamless SRTM data V4, International Centre for Tropical Agriculture (CIAT), 2008.
- Kim, H., Mnih, A., Schwarz, J., Garnelo, M., Eslami, A., Rosenbaum, D., Vinyals, O., and Teh, Y. W.: Attentive Neural 615 Processes, <https://doi.org/10.48550/ARXIV.1901.05761>, 2019.
- Lam, R., Sanchez-Gonzalez, A., Willson, M., Wirnsberger, P., Fortunato, M., Alet, F., Ravuri, S., Ewalds, T., Eaton-Rosen, Z., Hu, W., Merose, A., Hoyer, S., Holland, G., Vinyals, O., Stott, J., Pritzel, A., Mohamed, S., and Battaglia, P.: Learning skillful medium-range global weather forecasting, *Science*, 382, 1416–1421, <https://doi.org/10.1126/science.adi2336>, 2023.
- Lang, N., Jetz, W., Schindler, K., and Wegner, J. D.: A high-resolution canopy height model of the Earth, *Nat. Ecol. Evol.*, 620 7, 1778–1789, <https://doi.org/10.1038/s41559-023-02206-6>, 2023.



- Li, J. and Heap, A. D.: Spatial interpolation methods applied in the environmental sciences: A review, *Environ. Model. Softw.*, 53, 173–189, <https://doi.org/10.1016/j.envsoft.2013.12.008>, 2014.
- Moldovan, G., Pinnington, E., Nemesio, A. P., Lang, S., Bouallègue, Z. B., Dramsch, J., Alexe, M., Cruz, M. S., Hahner, S., Cook, H., Theissen, H., Clare, M., O'Brien, C., Polster, J., Magnusson, L., Mertes, G., Pinault, F., Raoult, B., Rosnay, P. de, 625 Forbes, R., and Chantry, M.: An update to ECMWF's machine-learned weather forecast model AIFS, <https://doi.org/10.48550/arXiv.2509.18994>, 23 September 2025.
- Pedregosa, F., Varoquaux, G., Gramfort, A., Michel, V., Thirion, B., Grisel, O., Blondel, M., Prettenhofer, P., Weiss, R., Dubourg, V., Vanderplas, J., Passos, A., Cournapeau, D., Brucher, M., Perrot, M., and Duchesnay, E.: Scikit-learn: Machine Learning in Python, *J. Mach. Learn. Res.*, 12, 2825–2830, 2011.
- 630 Reichstein, M., Camps-Valls, G., Stevens, B., Jung, M., Denzler, J., Carvalhais, N., and Prabhat: Deep learning and process understanding for data-driven Earth system science, *Nature*, 566, 195–204, <https://doi.org/10.1038/s41586-019-0912-1>, 2019.
- Sekulić, A., Kilibarda, M., Protić, D., and Bajat, B.: A high-resolution daily gridded meteorological dataset for Serbia made by Random Forest Spatial Interpolation, *Sci. Data*, 8, 123, <https://doi.org/10.1038/s41597-021-00901-2>, 2021.
- 635 Vaswani, A., Shazeer, N., Parmar, N., Uszkoreit, J., Jones, L., Gomez, A. N., Kaiser, L., and Polosukhin, I.: Attention Is All You Need, <https://doi.org/10.48550/ARXIV.1706.03762>, 2017.
- Vaughan, A., Tebbutt, W., Hosking, J. S., and Turner, R. E.: Convolutional conditional neural processes for local climate downscaling, *Geosci. Model Dev.*, 15, 251–268, <https://doi.org/10.5194/gmd-15-251-2022>, 2022.